ISSN 1063-7737, Astronomy Letters, 2017, Vol. 43, No. 4, pp. 221–232. © Pleiades Publishing, Inc., 2017.
Original Russian Text © L.I. Matveyenko, S.V. Seleznev, 2017, published in Pis'ma v Astronomicheskii Zhurnal, 2017, Vol. 43, No. 4, pp. 254–266.

# Active Zone of the Nucleus of the Quasar 3C 273

**L. I. Matveyenko*** **and S. V. Seleznev**

*Space Research Institute, Russian Academy of Sciences, Profsoyuznaya ul. 84/32, Moscow, 117997 Russia*

Received November 9, 2016

**Abstract**—The superfine structure of the quasar 3C 273 has been investigated at wavelengths $\lambda = 2$ and 6 cm with angular resolutions up to $\varphi = 20$ $\mu$as for epochs 2005–2014. We have identified a nozzle and a bipolar outflow: a jet and a counterjet consisting of coaxial high- and low-velocity components. The separation between the nozzles in the plane of the sky is $\Delta\rho = 0.84 \pm 0.16$ pc; the flow ejection velocity is $v \leqslant 0.1c$. The nozzle brightness temperature reaches $T_\mathrm{b} \approx 45 \times 10^{12}$ K, $\varphi = 20$ $\mu$as, $\lambda = 2$ cm. The ejected electrons radiatively cool at a distance up to $\leqslant$4 pc. However, the jet afterglow is observed at a 8% level at a distance up to $\rho \approx 16$ pc; the acceleration compensates for the radiative losses. The reduction in the emission level of the central flow at large distances determines the jet bifurcation. The counterjet shape is a mirror reflection of the initial part of the jet, suggesting a symmetry and identity of the ejected flows. The counterjet and jet nozzles are in the near and remote parts of the active region, respectively. The emission from the nozzles is absorbed by a factor of 2 and 15, respectively. The absorption decreases with increasing distance and the brightness of the jet fragments rises to its maximum at 0.5 pc from the nozzle. Arclike structures, arm fragments, are observed in the region of the nozzles. The relativistic plasma comes to the nozzles and is ejected. The brightness temperature of the arclike structures reaches 10% of the peak value, which is determined by the a smaller optical depth, the visibility in the transverse direction. The central high-velocity flow is surrounded by low-velocity components, hollow tubes being ejected as an excess angular momentum is accumulated. The remainder of the material flows along the arms toward the disk center until the next accumulation of an excess angular momentum and the process is repeated. The diameter of the outer nozzle is $\varnothing = 25$ pc and, further out, decreases exponentially; $\varnothing_n \approx 80\exp(-1.15n)$ pc. The flow kinematics, collimation, and acceleration have a vortical nature. Ring currents producing magnetic fields, which accelerate and stabilize the processes, are generated in the rotating flows (tubes). The tangential directions of the currents are observed as parallel chains of components.

**DOI:** 10.1134/S1063773717040053

Keywords: *quasar 3C 273, AGNs, jets, kinematics, vortices.*

## INTRODUCTION

The radio source 3C 273, one of the nearest ($z \approx 0.16$) and brightest ($m \approx 13$, https://ru.wikipedia.org/wiki/3C_273-cite_note-NED-3) objects, is located in the constellation Virgo. The distance to it is 748 Mpc, and its linear sizes correspond to 2.7 pc/mas. A compact source (quasar) and a one-sided jet are observed in the object. In radio emission at a wavelength of 75 cm the jet sizes reach 25″. According to the Hubble Space Telescope observations, the jet extent at optical wavelengths reaches a similar value of 23″ or ∼62 kpc (Uchiama et al. 2006). Observations of the lunar occultation of the source in Australia, Parkes, at 73 cm (Hazard et al. 1963) and at the Deep Space Network in Yevpatoria at 32 and 8 cm (Sholomitskii et al. 1965) allowed one to identify a compact source, a quasar, responsible for the high-frequency excess in the spectrum and to determine the spectral index of the jet $\alpha = -0.65$. Subsequent studies established a high activity of the quasar responsible for the variability of its radio emission (Dent and Haddock 1965; Kellermann et al. 1968; Matveyenko 1968). The synchrotron emission is determined by relativistic electrons. The emission changes in the entire spectrum of wavelengths from radio to gamma rays. The duration of radio outbursts is occasionally twice that of the quiescent emission level. The variability time scale lies within the range from several days to tens of days, which corresponds to exceptionally small angular sizes of the outflow region, $\leqslant$0.1 mas. The radio emission from outbursts lags behind with increasing wavelength, suggesting a large optical depth up to short centimeter wavelengths (Matveyenko 1983).

*E-mail: lmatveenko@gmail.com

The high activity suggests a complex structure of the nucleus of the object being investigated and touches on the mechanism of generation and ejection of flows of relativistic particles. The structure and developmental kinematics of the object are the most informative source of information about its nature. The factor that restrains the solution of the problem is the compactness of active nuclei. The method of very long baseline interferometry (VLBI) made this possible (Matveyenko et al. 1965; Matveyenko 2007). An active region, a bright compact source with a quasar whose brightness temperature at $\lambda = 2.8$ cm reached a limiting value of $T_b \approx 10^{12}$ K, was identified (Broderick et al. 1971; Cohen et al. 1977). The motion of compact knots in the jet with an apparent speed reaching $15c$ was detected. Observations at subsequent epochs at $\lambda = 1.35$ cm established the coincidence of the positions of the components, which caused a certain contradiction (Kellermann et al. 1968; Matveyenko and Pauliny-Toth 1978).

The explanation of the jet one-sidedness by a highly beamed emission from flow fragments moving with a relativistic velocity toward the observer also cause certain difficulties. This rules out the counterjet visibility but inevitably restricts the probability of visibility of the jet itself. Certain difficulties also arise with the energy source and with the exceptionally high efficiency of the electron acceleration mechanism for a very short time.

The short lifetime of outbursts makes it difficult to identify the fragments at different epochs of observations in the course of evolution. A certain influence is also exerted by the absorption of emission in the surrounding thermal plasma. Studies of quasars, in particular, the quasar 3C 345, have shown that the nuclei of galaxies are surrounded by a thermal plasma absorbing the radio emission from the active region (Matveyenko 2013). The transparency of this medium becomes sufficiently high only in the range of short centimeter and millimeter wavelengths. Some progress has been achieved in monitoring the quasar 3C 345 at $\lambda = 7$ mm and 2 cm. The ejection of the bipolar outflow, a jet and a counterjet, has been established. The ejection velocity does not exceed $v \leqslant 0.06c$. At a distance of $\sim$1 pc from the nozzle the fragments are accelerated to $8c$ and move with this velocity up to 2 pc, whereupon the velocity decreases to its initial value (Matveyenko and Sivakon' 2013). The observed two-sided jet and the kinematics of its motion suggest an explanation of the superluminal speeds by the refraction of the emission passing through the surrounding thermal plasma. Studies of the fine structure of several objects with active nuclei have established their vortical nature. The surrounding thermal plasma inflows onto the disk, is transferred along the spiral arms to the center, heats up, and is ejected as a bipolar outflow as an excess angular momentum is accumulated (Matveyenko et al. 2012, 2014, 2016). In this paper we report the results of our study of the fine structure of the active region in the quasar 3C 273 at wavelengths $\lambda = 2$ and 6 cm with an optimal angular resolution at epochs 2005–2014.

## STUDIES OF THE SUPERFINE STRUCTURE OF THE NUCLEUS OF THE QUASAR 3C 273

We studied the superfine structure of the quasar 3C 273 at $\lambda = 2$ and 6 cm based on NRAO VLBI archival data. Radio maps with optimal angular resolutions up to 20 $\mu$as were obtained for epochs 2005–2014. A bright compact component (nozzle), a bipolar outflow including a central high-velocity component and surrounding low-velocity components (Figs. 1a–1e, the resolutions are 0.01 and 0.05 mas), and an active region on an enlarged scale (Fig. 2, the resolution is 0.05 mas) are identified in the structure. The bipolar outflow is oriented in a direction of 47°. Let us consider the peculiarities of the structure at these epochs.

### *Low-Velocity Bipolar Outflows*

A central active region and a bipolar outflow including a jet and a counterjet are identified in the structure of the quasar (Fig. 1). The orientation of the outflow corresponds to 47°. The coaxial structure of the outflow consists of central high-velocity and surrounding low-velocity components. The diameter of the outer low-velocity component $\varnothing = 3$ mas or 8 pc; it is observed up to 6 mas with its separation from the disk nozzle at 2 mas (5.4 pc), epochs 2007–2010, $\lambda = 2$ cm (Table 1 and Fig. 1). The separation is determined by the completion of the removal of an excess angular momentum and the lag of the accumulation of an excess angular momentum in the inflowing material. The attenuated emission in the

**Table 1.** Dependence of the jet nozzle diameter on $n$; $\varnothing_n = 54 \exp\{-0.76n\}$, pc

| $n$ | $\varnothing$, mas/pc | $\rho$, mas | $\varnothing_{calc}$, pc |
|---|---|---|---|
| 1 | 9.5/25 | 5–25 | 25 |
| 2 | 3/8 | 2–6 | 8 |
| 3 | 2/5.4 | 1.4–6 | 5.5 |
| 4 | 1.1/3 | 0–6 | 2.6 |
| 5 | 0.7/1.9 | 0–6 | 1.2 |

Observed with separation from the disk increasing with distance.

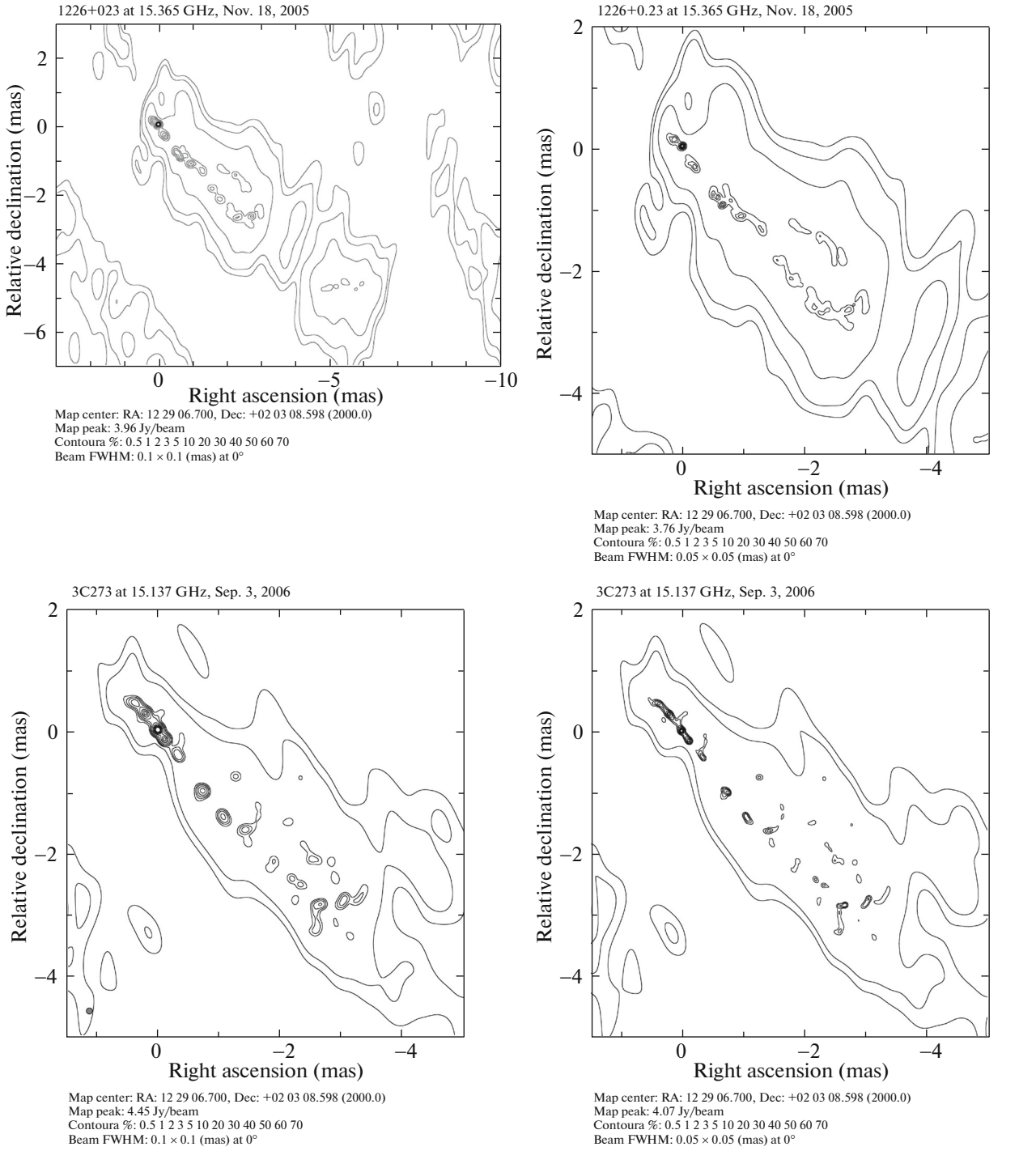


**Fig. 1.** Maps of the brightness distribution for the quasar 3C 273 at $\lambda = 2$, 3, and 6 cm, the resolutions are $\phi = 0.10$, 0.05, and 0.025 mas, respectively, epochs 2005–2014.

region under consideration emphasizes the inner low-velocity component with diameter $\varnothing = 2$ mas, 5.4 pc. In this case, the outflow separation is at 1.4 mas. The ejection of the low-velocity bipolar outflow with diameter $\varnothing = 1.1$ mas is observed completely from the nozzle exit at a distance $-1.5$ mas $\leqslant \rho \leqslant 1.5$ mas, epochs 2007 and 2008. Two parallel chains of components enclosing the central high-velocity outflow are identified in the jet region. The chains of components correspond to the tangential directions of the inner low-velocity outflow with diameter $\varnothing = 0.7$ mas, epoch 2008. The links of the chains correspond to the rings built into the outflow wall. The sizes of the links are $\sim$0.07 mas; their brightness is low and

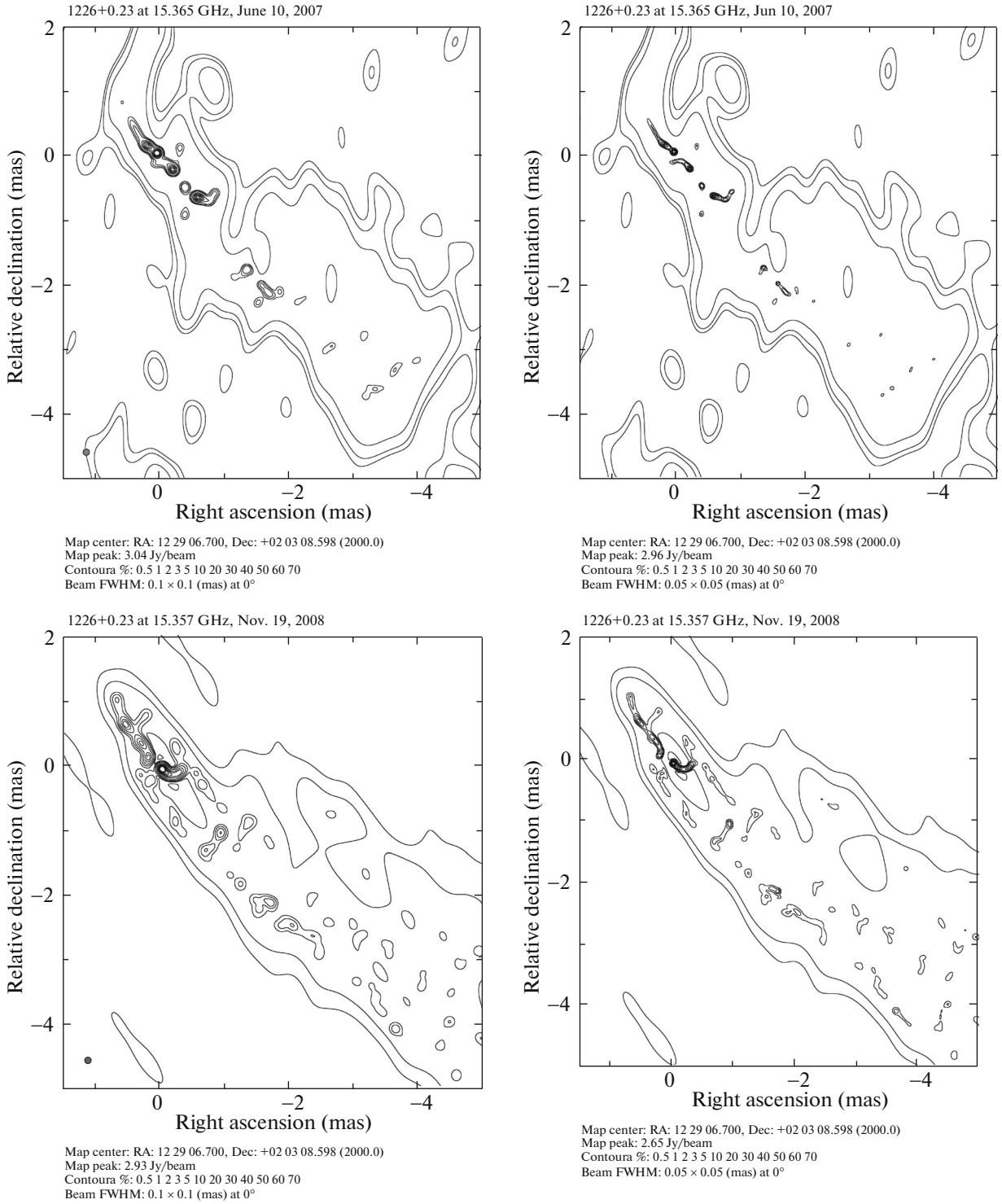


**Fig. 1.** (Contd.)

exceeds the background emission by a factor of 2–3. The brightness of the low-velocity components reaches 2% of the peak value, which corresponds to $T_b \approx 10^{13}$ K at the epochs under consideration at $\varphi =$ 0.05 mas.

Similar features are observed in the preceding period in the remote part of the disk, a nozzle with diameter $\varnothing \approx 9.5$ mas or 25 pc, at $\lambda = 6$ cm (Fig. 1e, epoch 2009, $\varphi = 0.1$ and 0.3 mas). The outflow is visible up to 25 mas or 70 pc, with its separation from the nozzle at 14 pc (Table 1). As previously, the

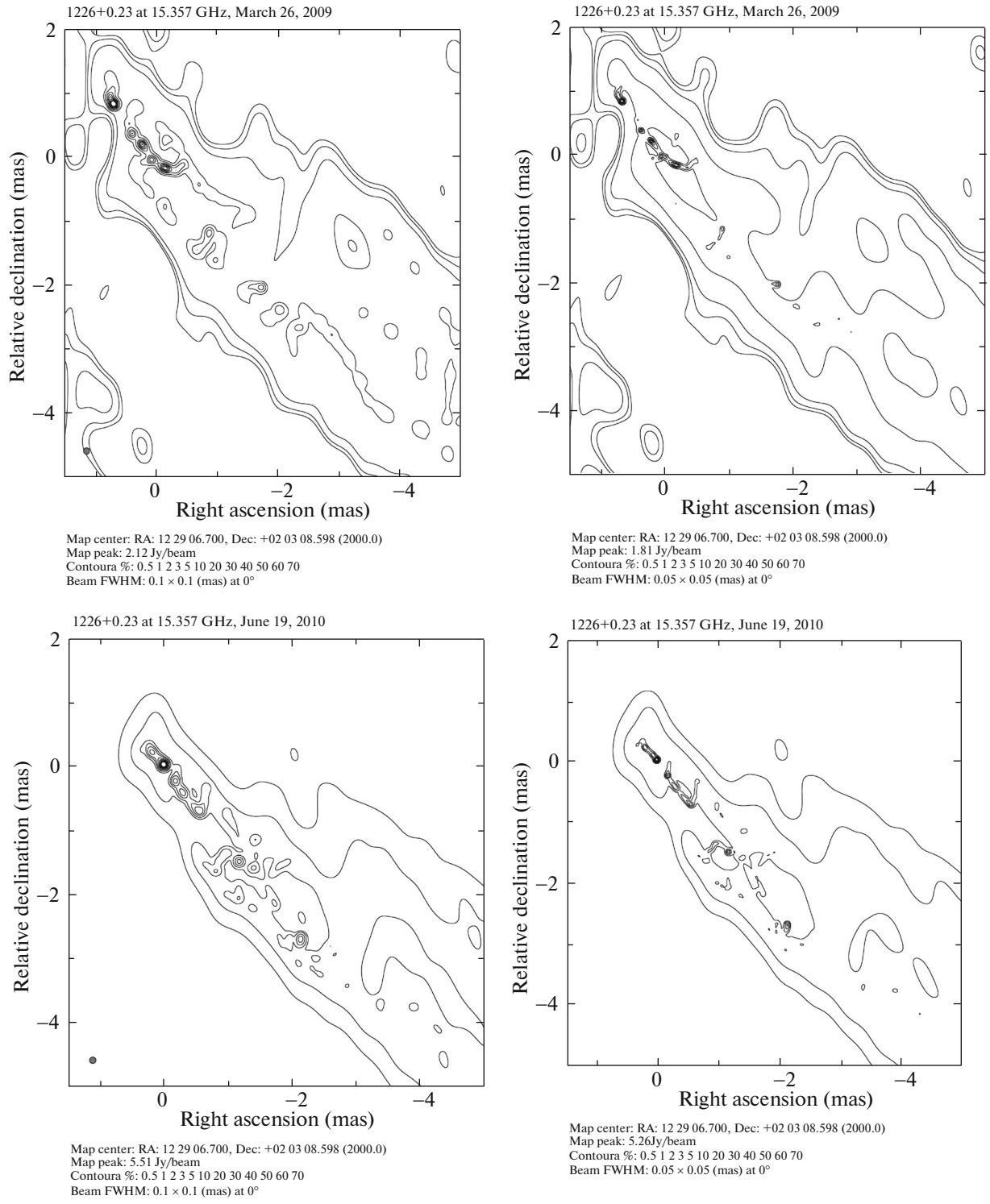


**Fig. 1.** (Contd.)

brightness temperature of the outflow did not exceed 2% of the peak value, $T_b \approx 17 \times 10^{12}$ K.

*High-Velocity Bipolar Outflow*

Studies of the superfine structure of several AGNs have established that the ejection of the flows of matter occurs symmetrically and corresponds to a two-sided jet. The flows include coaxial low-velocity components surrounding a central high-velocity outflow. The velocity and brightness of the flows increase as the center is approached (Matveyenko 2016). For the quasar 3C 273 at $\lambda = 2$ cm the relative intensities of

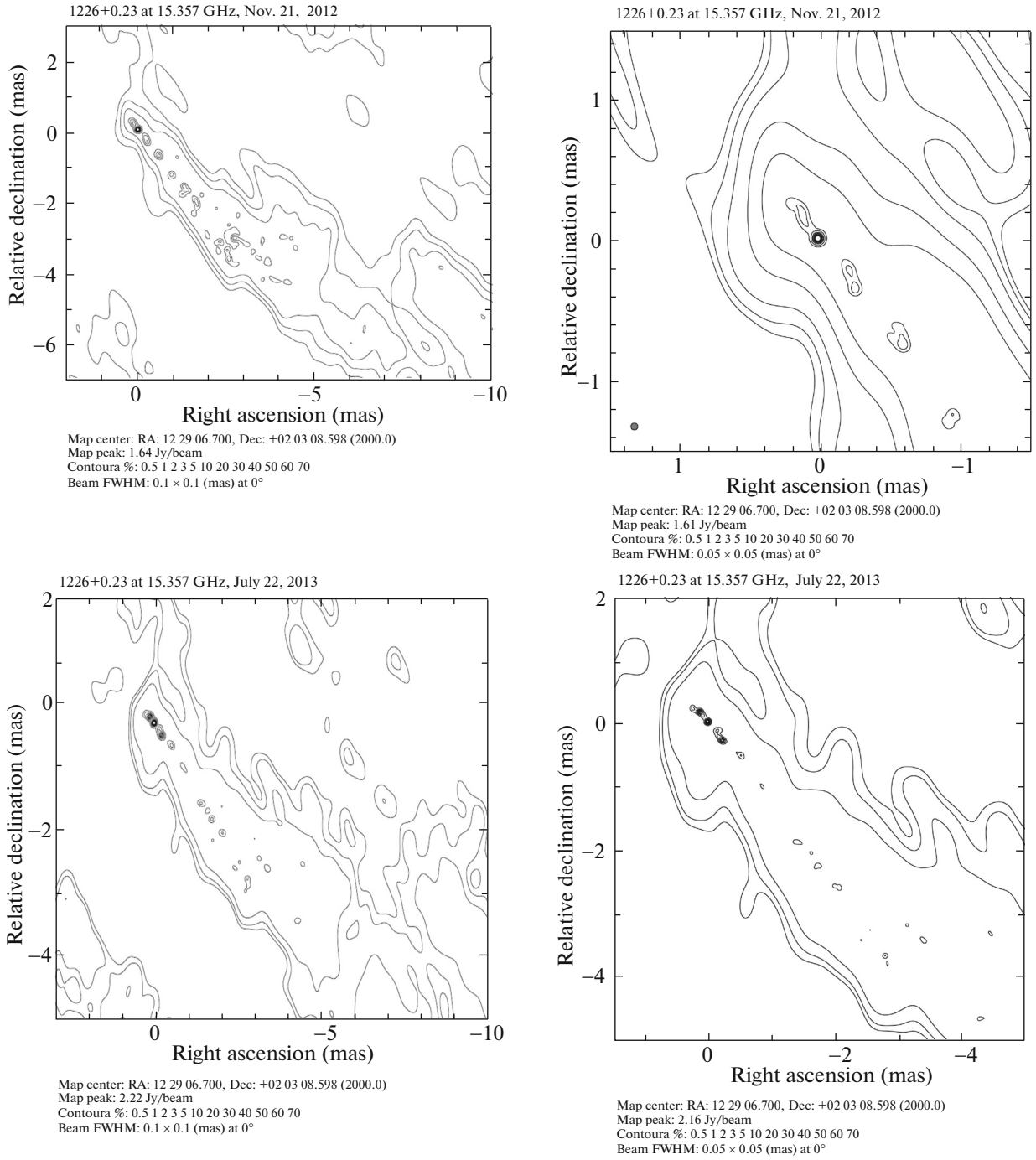


**Fig. 1.** (Contd.)

the flows are low, within a few percent of the peak value. To a certain extent this is also true for the high-velocity central bipolar outflow. The brightest part of the outflow is observed at relatively small distances, $-1.5$ mas $\leqslant \rho \leqslant 1.5$ mas. At epochs 2006–2008 the counterjet emission dominates (Fig. 1). At $\lambda = 6$ cm the fragments of the high-velocity bipolar outflow are observed at distances up to 2 mas in the counterjet and 3 mas in the jet, epoch 2009, the resolutions are 0.1 and 0.3 mas (Fig. 1e). The reduced emission from the central jet at a large distance explains the bifurcation of the outflow, whose fragments correspond to the tangential directions of the low-velocity components (Fig. 1e, epoch 2009).

### *Brightness of the Bipolar Outflow*

The changes in the relative brightness of the fragments of the bipolar outflow, the jet and counterjet,

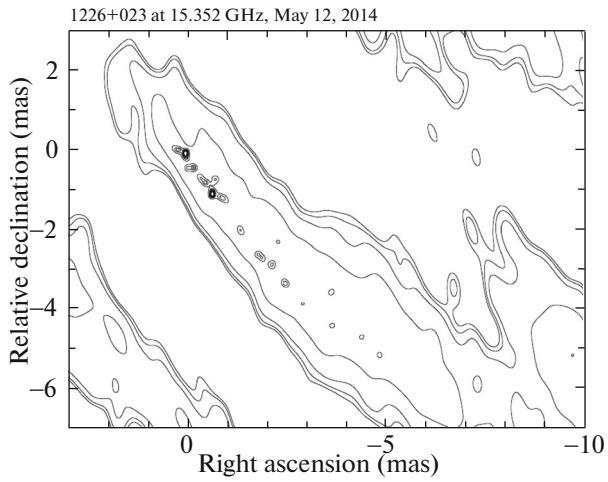


Map center: RA: 12 29 06.700, Dec: +02 03 08.598 (2000.0)
Map peak: 1.13 Jy/beam
Contoura %: 0.5 1 2 3 5 10 20 30 40 50 60 70
Beam FWHM: 0.1 × 0.1 (mas) at 0°

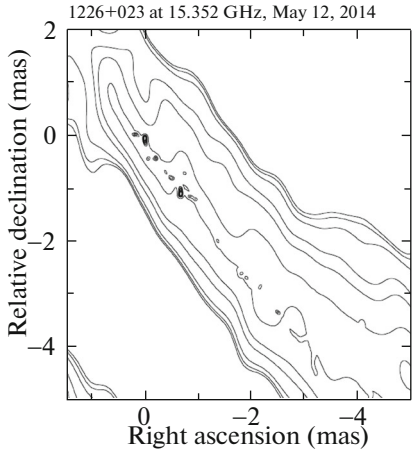


Map center: RA: 12 29 06.700, Dec: +02 03 08.598 (2000.0)
Map peak: 0.748 Jy/beam
Contoura %: 0.5 1 2 3 5 10 20 30 40 50 60 70
Beam FWHM: 0.05 × 0.05 (mas) at 0°

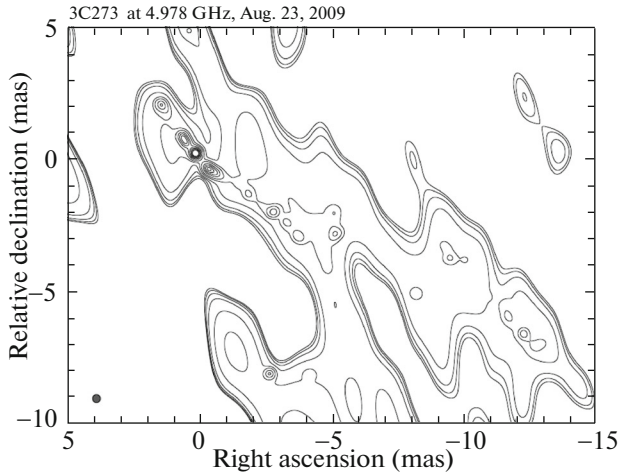


Map center: RA: 12 29 06.700, Dec: +02 03 08.598 (2000.0)
Map peak: 2.59 Jy/beam
Contoura %: 0.5 1 2 3 5 10 20 30 40 50 60 70
Beam FWHM: 0.3 × 0.3 (mas) at 0°

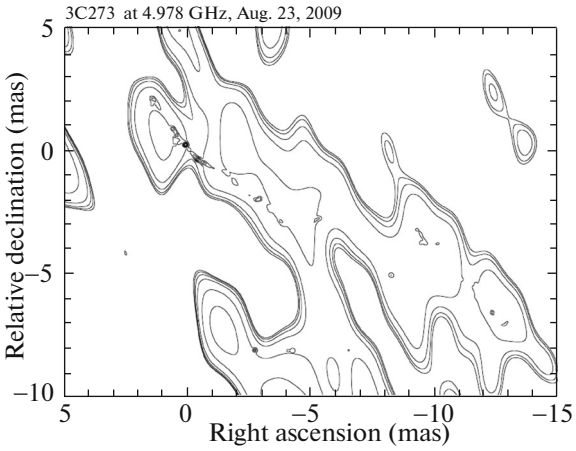


Map center: RA: 12 29 06.700, Dec: +02 03 08.598 (2000.0)
Map peak: 2.32 Jy/beam
Contoura %: 0.5 1 2 3 5 10 20 30 40 50 60 70
Beam FWHM: 0.1 × 0.1 (mas) at 0°

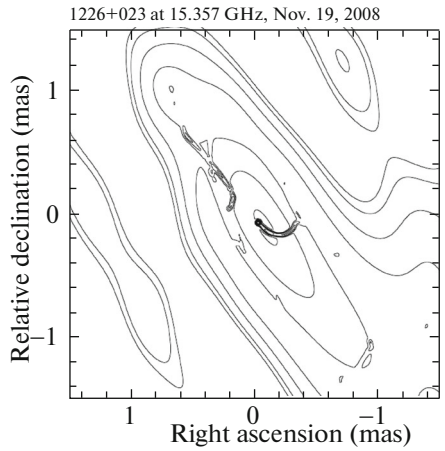


Map center: RA: 12 29 06.700, Dec: +02 03 08.598 (2000.0)
Map peak: 2.27 Jy/beam
Contoura %: 0.5 1 2 3 5 10 20 30 40 50 60 70
Beam FWHM: 0.02 × 0.02 (mas) at 0°

**Fig. 1.** (Contd.)

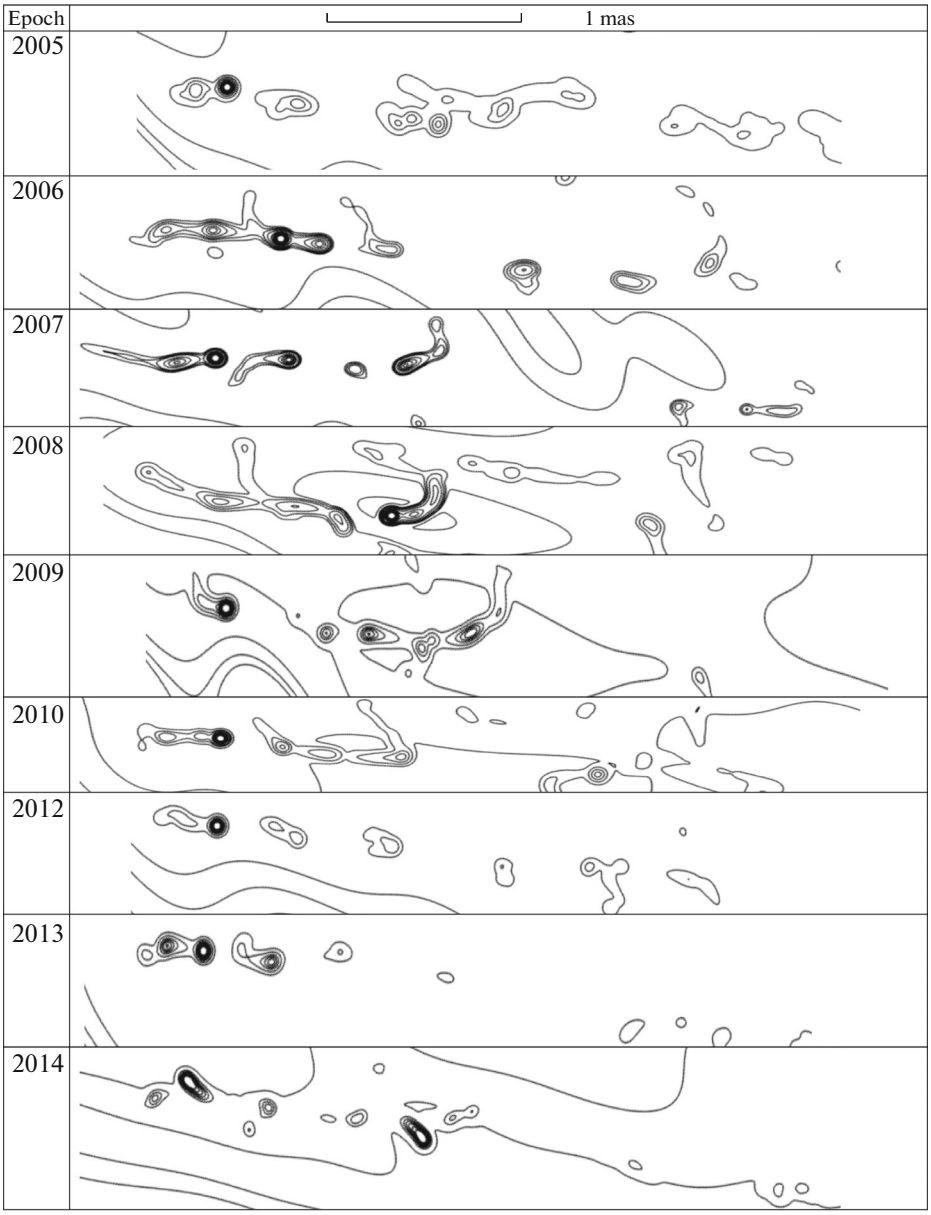


**Fig. 2.** Fine structure of the bipolar outflow of the quasar 3C 273, epochs 2005–2014. The resolution is Ø = 0.05 mas.

with distance $\rho$ in mas at $\lambda = 2$ cm, $\varphi = 50$ $\mu$as, are shown in Fig. 3 and given in Table 2. Unusual changes in brightness are observed at epochs 2007 and 2008. At epochs 2007 and 2008 the peak brightness corresponds to counterjet and jet fragments, respectively. The jet and counter nozzles are in the remote and near parts of the active region, respectively; therefore, the apparent brightness of the jet fragments increases as we go outside the absorbing screen. Having reached its maximum value, the brightness decreases exponentially at a distance $\rho \approx 0.6$ mas to a ≈10% level and, further out, remains at this level up to $\rho \approx 1.5$ mas. This suggests an acceleration of the outflow compensating for the radiative losses. The reduction in the emission from the central outflow of the jet at distances $\rho \geqslant 4$ mas leads to jet bifurcation (Fig. 1e, $\lambda = 6$ cm).

### *Arm Fragments*

Arclike fragments adjacent to the nozzles are identified in the fine structure of the active region of the quasar 3C 273 at epochs 2007–2009 (Fig. 1, $\varphi = 0.05$ and 0.1 mas). Similar fragments were first detected in the object 3C 454.3. These were shown to be fragments of the arms along which the surrounding material flows into the nozzles and is ejected as a bipolar outflow (Matveyenko 2016). In our case, these also correspond to spiral arm

**Table 2.** Relative positions of the bipolar outflow fragment measured from the counterjet nozzle "0" cm; $\rho = 0.4$ pc/cm

| $n$ | Date | | | | | | | | | Mean |
|---|---|---|---|---|---|---|---|---|---|---|
| | 18.11.05 | 3.09.06 | 10.10.07 | 19.11.08 | 26.03.09 | 19.01.10 | 21.11.12 | 22.07.13 | 12.05.14 | |
| | | | | | $\varphi = 0.05$ mas | | | | | |
| −5 | − | − | − | 3.1 | − | − | − | − | − | 3.1 |
| −4 | − | − | − | 2.2 | 2.3 | − | − | − | − | $2.25 \pm 0.05$ |
| −3 | − | 1.5 | 1.2 | 1.25 | 1.9 | − | − | − | − | $1.46 \pm 0.2$ |
| −2 | − | 0.85 | − | 0.65 | − | 0.7 | − | 0.75 | − | $0.74 \pm 0.1$ |
| −1 | 0.45 | − | 0.4 | − | − | 0.25 | 0.5 | 0.45 | 0.45 | $0.42 \pm 0.1$ |
| 0 | 0 | 0 | 0 | 0 | 0 | 0 | 0 | 0 | 0 | 0 |
| 1 | 0.7 | 0.5 | 0.4 | 0.6 | 0.7 | 0.8 | 0.8 | 0.6 | 0.6 | $0.63 \pm 0.1$ |
| 2 | 0.9 | − | 0.9 | − | − | − | − | 1.0 | 1.1 | $0.98 \pm 0.1$ |
| 3 | − | 1.35 | 1.2 | − | 1.35 | 1.25 | 1.15 | − | 1.9 | $1.37 \pm 0.2$ |
| 4 | 2.3 | − | 2.35 | − | 1.75 | 2.2 | 2.4 | 1.9 | 2.3 | $2.17 \pm 0.2$ |
| 5 | 2.85 | 3.1 | − | 3.4 | − | − | − | 3.4 | 3.0 | $3.15 \pm 0.2$ |
| 6 | 3.75 | − | − | − | − | − | 4.0 | − | 3.6 | $3.78 \pm 0.2$ |
| 7 | 4.6 | 4.4 | − | 4.2 | 4.4 | 4.8 | − | − | − | $4.48 \pm 0.2$ |
| 8 | − | 5.45 | 5.7 | − | − | 5.3 | 5.2 | − | − | $5.41 \pm 0.2$ |
| 9 | 6.1 | − | 6.5 | − | − | − | 5.6 | 5.9 | 6.0 | $6.02 \pm 0.2$ |
| 10 | 6.95 | 7.2 | 6.95 | 7.7 | 7.4 | − | 6.65 | 7.1 | − | $7.14 \pm 0.3$ |
| 11 | 8.4 | 8.25 | − | − | − | − | − | 8.3 | 7.85 | $8.2 \pm 0.2$ |
| 12 | 8.9 | 8.6 | − | 8.8 | 8.55 | 8.6 | − | − | 8.15 | $8.6 \pm 0.2$ |
| 13 | 9.6 | 9.7 | 10.05 | 10.05 | 9.65 | − | − | − | 9.0 | $9.68 \pm 0.3$ |
| 14 | − | − | − | − | − | − | 10.3 | − | 10.5 | $10.4 \pm 0.1$ |
| 15 | − | − | − | − | − | − | − | 11.05 | − | 11.05 |
| 16 | − | − | 12.5 | − | − | − | − | − | − | 12.5 |
| Cjet, % | 100 | 100 | 100 | 20 | 100 | 100 | 100 | 100 | 100 | − |
| Jet, % | 10 | 10 | 40 | 100 | 50 | 20 | 30 | 40 | 30 | − |
| | | | | | $\varphi = 0.1$ mas | | | | | |
| −5 | − | − | − | 3.2 | 2.85 | − | − | − | − | $3.03 \pm 0.2$ |
| −4 | − | − | − | 2.2 | 2.3 | − | − | − | 2.6 | $2.37 \pm 0.2$ |
| −3 | − | 1.45 | 1.3 | 1.45 | 1.95 | − | − | − | − | $1.54 \pm 0.2$ |
| −2 | − | 0.85 | − | 0.75 | 0.65 | 0.7 | 0.6 | 0.9 | − | $0.74 \pm 0.1$ |
| −1 | 0.4 | − | 0.5 | − | − | − | − | 0.55 | 0.5 | $0.49 \pm 0.04$ |
| 0 | 0 | 0 | 0 | 0 | 0 | 0 | 0 | 0 | 0 | 0 |
| 1 | − | 0.4 | − | 0.55 | 0.7 | 0.75 | 0.8 | 0.7 | 0.8 | $0.67 \pm 0.1$ |
| 2 | 0.95 | − | 0.9 | − | − | − | 1.1 | 0.95 | 1.0 | $0.98 \pm 0.1$ |
| 3 | − | 1.25 | 1.35 | − | 1.3 | 1.25 | − | 1.8 | 1.8 | $1.46 \pm 0.2$ |
| 4 | 2.45 | − | 2.45 | − | 2.0 | 2.25 | 2.35 | − | 2.5 | $2.33 \pm 0.1$ |
| 5 | 2.95 | 3.05 | − | 3.25 | − | − | − | 3.5 | 3.0 | $3.15 \pm 0.2$ |
| 6 | 3.7 | − | − | − | − | − | 4.0 | − | 3.6 | $3.77 \pm 0.2$ |
| 7 | 4.6 | 4.4 | − | 4.1 | 4.35 | 4.7 | − | − | − | $4.43 \pm 0.2$ |
| 8 | − | 5.4 | 5.5 | 5.35 | 5.3 | 5.35 | 5.35 | 5.8 | 5.95 | $5.5 \pm 0.2$ |
| 9 | 6.25 | − | 6.6 | 6.5 | − | − | 6.55 | 6.55 | − | $6.49 \pm 0.1$ |
| 10 | 7.15 | 7.2 | 6.95 | 7.65 | 7.4 | 6.85 | − | 7.1 | 7.25 | $7.19 \pm 0.2$ |
| 11 | 8.1 | 8.15 | − | − | − | − | − | 8.35 | 7.9 | $8.13 \pm 0.1$ |
| 12 | 9.0 | 8.5 | − | − | 8.6 | 8.65 | − | − | 8.85 | $8.72 \pm 0.2$ |
| 13 | 9.6 | 9.7 | − | − | 9.65 | − | 9.7 | − | − | $9.66 \pm 0.04$ |
| 14 | 10.15 | − | 10.15 | − | − | − | 10.3 | 10.45 | 10.25 | $10.26 \pm 0.1$ |
| 15 | − | − | − | − | − | 11.2 | − | 11.55 | 12.0 | $11.58 \pm 0.3$ |
| 16 | − | − | 12.5 | − | − | − | − | − | 12.85 | $12.68 \pm 0.2$ |
| $I_\circ$ | 3.9/3.1 | 4.5/3.6 | 3.0/2.4 | 2.9/2.3 | 2.1/1.7 | 5.5/4.4 | 1.8/1.4 | 2.3/1.8 | 1.1/0.9 | Jy/beam/$10^{12}$ |
| Cjet, % | 100 | 100 | 80 | 40 | 100 | 100 | 100 | 100 | 100 | Nozzle |
| Jet, % | 10 | 30 | 100 | 100 | 40 | 20 | 10 | 40 | 30 | Nozzle |

The separation between the nozzles is 0.63 cm (or 0.25 mas or 0.768 pc; 1 mas = 2.5 cm); $\rho = 2.7$ pc/mas.

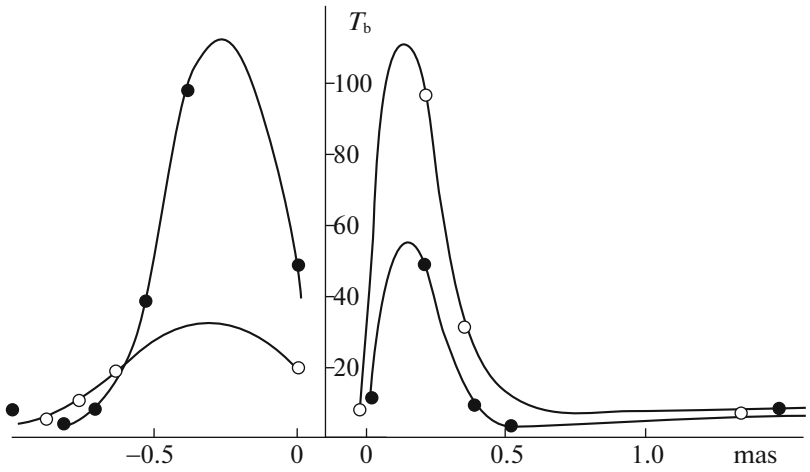


**Fig. 3.** Brightness distribution in the high-velocity bipolar outflow of the quasar 3C 273, the resolution is $\rho = 0.05$ mas, epochs 2007 (● - ● - ● - ●) and 2008 (○ - ○ - ○ - ○).

fragments. Their sizes reach 0.4 mas in length or ≈10 pc. The superfine structure of the region with resolution $\varphi = 0.02$ mas at epoch 2008 is presented in Fig. 1e. The brightness temperature of the outflow fragment at the exit from the jet nozzle reaches $T_b \approx 45 \times 10^{12}$ K. The brightness temperature of the arm fragments reaches 10% of the peak value and is $T_b \approx 5 \times 10^{12}$ K. The relativistic plasma flows along the arms to the nozzles and is ejected in directions of 40° (counterjet) and 140° (jet) in the plane of the sky. The reduced brightness of the arm fragments observed in the transverse direction is determined by a smaller optical depth than that of the nozzle.

### *Nozzles*

The observed bright source corresponding to the counterjet nozzle is located in the part of the active region nearest to the observer. The jet nozzle is in the opposite, remote part and its emission is attenuated by absorption in this region. The separation between the nozzles in the plane of the sky is $\Delta\rho = 0.31 \pm 0.06$ mas or $0.84 \pm 0.16$ pc (Fig. 1). The brightness of the jet nozzle in comparison with the counterjet is, on average, 20% (Table 2). As the outflow fragments recede from the nozzle, absorption is reduced and the brightness rises. At $\rho \geqslant 0.25$ mas the brightness reaches 70% of its peak value, epochs 2007–2009.

### *Kinematics of the Bipolar Outflow Fragments*

Let us consider the positions of the outflow fragments at various epochs. We will take the bright compact source (counterjet nozzle) as a reference source. The relative positions of the jet and counterjet fragments $\rho$ in arbitrary units in the period under consideration are given in Table 2; the resolution is 0.1 and 0.05 mas, respectively. Recalculating the positions of the components in arbitrary units corresponds to $1.08\rho$ pc. The negative and positive values refer to the counterjet and jet, respectively. Table 2 gives the mean positions of the components. The positions of the components nearest to the nozzle as a function of time remain within ±0.1 mas, or ±0.3 pc. The remote components of the jet can be below the detection limit, but if they are present, then their positions remain within ±0.2 or ± 0.5 pc. The observed small differences in the positions of the components at different resolutions are determined by their fine structure. No regular changes in the positions of the compact jet and counterjet components during the period under consideration within 0.3–0.5 pc are observed. On the basis of these limits, the apparent velocities of the components in the plane of the sky over the 9-year period under consideration correspond to $v \leqslant 0.1c$ and $v \leqslant 0.17c$ for the near and remote parts of the jet, respectively.

## DISCUSSION

In the period 2005–2014 under consideration both jet and counterjet are observed in the structure of the quasar 3C 273 at $\lambda = 2$ cm. The shape of the counterjet is a mirror reflection of the initial part of the jet, suggesting a symmetry and identity of the ejected flows (Fig. 1). The structure of the bipolar outflow changes only slightly. The observed changes in the brightness of the components are determined mainly by the discreteness of the isophotes (Fig. 1). The separation between the nozzles in the plane of the sky is $\Delta\rho = 0.84 \pm 0.16$ pc. The nozzles are spaced apart in a direction oriented at an angle of 50°. The peculiarities of the superfine structure manifest themselves at epochs 2007 and 2008 (Figs. 1 and 2).

**Table 3.** Brightness distribution in the bipolar outflow, %; epochs 2007 and 2008, $\varphi = 50$ $\mu$as

| $\rho$, mas | Brightness, % | $\rho$, mas | Brightness, % |
|---|---|---|---|
| 2007 | | 2008 | |
| −1 | 5 | – | – |
| −0.8 | 7 | −1.0 | 10 |
| −0.6 | 40 | −0.86 | 5 |
| −0.4 | 100 | −0.60 | 20 |
| – | 50 | −0 | 20 |
| +0 | 10 | +0 | 20 |
| 0.26 | 50 | 0.2 | 100 |
| 0.46 | 10 | 0.31 | 30 |
| 0.61 | 7 | 0.47 | 20 |
| 1.7 | 10 | 1.5 | 10 |

The brightnesses of the fragments at the exit from the near (counterjet) and remote (jet) nozzles at epoch 2007 are 50 and 7% of the peak value, respectively. At a brightness of the fragments corresponding to the peak value, the observed difference suggests the absorption of emission by a factor of 2 and 15, respectively. The absorption is reduced as the outflow fragments recede. The brightness of the jet fragment rises to its maximum at 0.5 pc from the nozzle.

Arclike structures are observed in the central region of the quasar near the nozzles (epochs 2007–2009, Figs. 1 and 2). The superfine structure with a resolution of 0.02 mas (epoch 2008) is presented in Fig. 1e. The arcs correspond to the fragments of the arms along which the relativistic plasma flows into the nozzles and is ejected as high-velocity outflows. The apparent brightness temperature of the inflowing plasma reaches $T_\mathrm{b} \approx 5 \times 10^{12}$ K and is higher by an order of magnitude at the exit from the nozzles: $T_\mathrm{b} \approx 45 \times 10^{12}$ K. This difference is determined by the smaller optical depth of the arm observed in the transverse direction. The flow ejection velocity is $v \leqslant 0.1c$.

As the thermal plasma flows to the center, it is heated and accelerated. The brightness temperatures of the outflow at the exit from the nozzle in the period under consideration at resolution $\varphi = 0.05$ mas are $2 \times 10^{12}$ K $\leqslant T_\mathrm{b} \leqslant 17 \times 10^{12}$ K. At resolution $\varphi =$ 20 $\mu$as the brightness temperature at the exit from the nozzle reaches $T_\mathrm{b} \approx 45 \times 10^{12}$ K (the epoch November 19, 2008a).

The fine structure of the active region in the flow ejection region is complex and undergoes fairly rapid changes in the period 2007–2008. To a first approximation, we may consider it as bipolar outflow fragments. The counterjet and jet brightnesses decrease exponentially to a level of several percent at $\rho \approx 0.7$ mas or $\approx$2 pc, which is determined by the radiative cooling time of the ejected relativistic electrons (Fig. 3, epochs 2007 and 2008; Table 3). It follows from the figure that the dependences change places jet–counterjet. However, the counterjet extent at both epochs exceeds the jet extent by a factor of $\approx$1.5, while the jet emission continues to be observed at a $\sim$8% level at a distance up to $\rho \approx 4$ pc. The afterglow is determined by the acceleration of the outflow compensating for the radiative losses of relativistic electrons. This emission belongs to the remote part of the jet and does not depend on the observed changes at the epochs under consideration.

The central high-velocity outflow is surrounded by low-velocity components, hollow tubes ejected as an excess angular momentum is accumulated. The ejection ceases as an excess angular momentum is carried away; the separation of the low-velocity outflow from the nozzle observed as steps in the extended component occurs. The remainder of the material continues to flow along the arm to the disk center until an excess angular momentum is accumulated and the process is repeated. The diameter of the outer outflow (nozzle) observed at 6 cm is $Ø_1 \approx 9.5$ mas (25 pc), further out, $Ø_2 \approx 3$ mas (8 pc), $Ø_3 \approx 0.9$ mas (2.5 pc), and $Ø_4 \approx 0.7$ mas at a wavelength of 2 cm

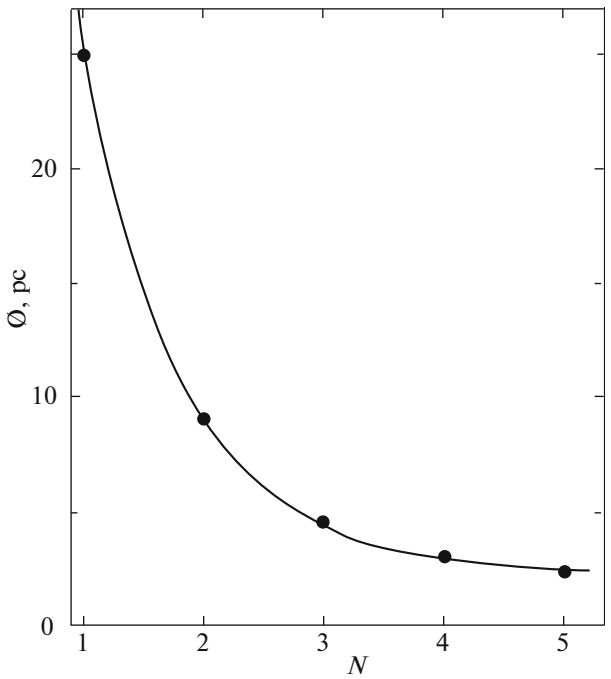


**Fig. 4.** Diameters of the nozzle of the bipolar outflow of the quasar 3C 273 versus distance to the center.

(Table 1, $n$ is the number counted from the outer nozzle). The diameters of the nozzles decrease exponentially: $\varnothing_n \approx 80\exp(-1.15n)$ pc. The observed features, the collimation and acceleration of the outflows correspond to vortex hydrodynamics (Abrahamyan and Matveyenko 2012).

The emission from the low-velocity jet outflow is insignificant, it does not exceed a few percent of the peak value, but it is observed at fairly large distances. The emission from the central high-velocity outflow is reduced faster and at distances $\rho \geqslant 16$ pc falls to a level below that of the low-velocity components, which leads to the jet bifurcation observed at $\lambda = 6$ cm (Fig. 1e). Ring currents whose tangential directions are observed as parallel chains of components are generated in the walls of the rotating tubes. The ring currents produce solenoidal magnetic fields.

## CONCLUSIONS

The fine structure of the quasar 3C 273 is typical of AGNs and has a vortical nature. The thermal plasma of the surrounding medium flows to the vortex, heats up, is accelerated, and is transferred along the arms to the center. As an excess angular momentum is accumulated, it is carried away by the rotating bipolar outflow. The diameters of the nozzles correspond to an exponential dependence $\varnothing_n \approx 80\exp(-1.15n)$ pc. A high-velocity outflow surrounded by low-velocity components is formed. The separation of the low-velocity jet components is determined by the reduction in the inflow of material, which can be determined by the increase in the velocity of the material as the disk center is approached or by the old age of the galaxy. Ring currents producing the magnetic fields of the structures are generated in the rotating outflows. The outflow velocities are $v \leqslant 0.1c$ in the ejection region and $v \leqslant 0.17c$ in the remote part. The brightness temperature of the relativistic electrons reaches $T_\mathrm{b} = 5 \times 10^{13}$ K. The kinematics of their motion determines the collimation and acceleration of the outflows, along with the generation of a magnetic field. The gravitational field of the forming central body, a black hole, stabilizes and accelerates the process.

## ACKNOWLEDGMENTS

This work was supported by the Basic Research Program P-7 of the Presidium of the Russian Academy of Sciences, the "Transitional and Explosive Processes in Astrophysics" subprogram, and the Program of the Division of Physical Sciences.

## REFERENCES

1. M. G. Abramyan and L. I. Matveyenko, Astrofizika **3**, 397 (2012).
2. D. D. Broderik et al., Sov. Astron. **14**, 627 (1970).
3. M. H. Cohen, R. P. Linfield, A. T. Moffet, G.A. Seielstad, K. I. Kellermann, D. B. Shaffer, et al., Nature **268**, 405 (1977).
4. W. A. Dent and T. T. Hadbeck, Nature **205**, 4970 (1965).
5. C. Hazard, M. B. Mackey, and A. J. Shimmins, Nature **197**, 1037 (1963).
6. K. I. Kellermann and I. I. K. Pauliny-Toth, Ann. Rev. Astron. Astrophys. **6**, 417 (1968).
7. L. I. Matveyenko, Sov. Phys. Usp. **26**, 612 (1983).
8. L. I. Matveyenko, Astron. Nachr. **328**, 411 (2007).
9. L. I. Matveyenko, ICR Preprint 2179 (Inst. Cosm. Res., Moscow, 2016a).
10. L. I. Matveyenko, in *Proceedings of the 13th EVN Symposium and Users Meeting* (2016b, in press).
11. L. I. Matveyenko and S. S. Sivakon', Astron. Lett. **39**, 481 (2013).
12. L. I. Matveyenko et al., Izv. Vyssh. Uchebn. Zaved., Radiofiz. **5**, 682 (1968).
13. L. I. Matveyenko et al., Sov. Astron. **17**, 731 (1973).
14. L. I. Matveyenko, D. A. Graham, and J. T. Zensus, Astron. Rep. **49**, 259 (2005).
15. I. I. K. Pauliny-Toth, E. Preuss, A. Witzel, et al., Sov. Astron. Lett. **4**, 32 (1978).
16. G. B. Sholomitskii, N. F. Sleptsova, and L. I. Matveyenko, Sov. Astron. **9**, 882 (1965).
17. Y. Uchiyama, C. M. Urry, C. C. Cheung, S. Jester, J. van Duyne, P. Coppi, R. M. Sambruna, T. Takahashi, F. Tavecchio, and L. Maraschi, Astrophys. J. **648**, 910 (2006).

*Translated by G. Rudnitskii*